

Prevention and Treatment of Natural Disasters

https://ojs.ukscip.com/index.php/ptnd

Article

HVSR Survey Along the Wasatch Fault (Provo Segment)

Kathryn J. Smith 1 0 , John McBride 2,* 0 , Stephen T. Nelson 3 0 , Ronald A. Harris 2 0 , Kevin A. Rey 2 0 and Bo Worthen 2

Received: 13 September 2025; Revised: 27 October 2025; Accepted: 27 October 2025; Published: 14 November 2025

Abstract: The Wasatch Fault Corridor in northern Utah (USA) faces increasing seismic risks due to rising population density. V_{s30} is a vital parameter for understanding how a site will respond to earthquake shaking; however, obtaining V_{s30} can be costly or impractical because of infrastructure or access challenges. The horizontal-to-vertical spectral ratio (HVSR) enables rapid assessment, provided a relationship between V_{s30} and the resonant frequency (f_0) of the shallow subsurface can be established. Previously surveyed V_{s30} sites in the Provo segment of the Wasatch Fault Zone were measured with a three-component seismometer to obtain f_0 . These sites are located on the hanging wall of the fault zone, within alluvial and lacustrine Quaternary sediments. For each of the 20 sites, ambient noise was recorded for 30 minutes and amplitude-frequency spectra computed for each component. A rubric was applied to select site results most suitable for analysis and forward modelling, based on uncertainty of f_0 , uncertainty of f_0 , uncertainty of f_0 , which ranged from 0.28 to 1.38 Hz. Experimenting with linear regression helps guide understanding of the potential for estimating f_0 from HVSR in this region.

Keywords: Ambient Noise; Seismic Hazard; Spectral Analysis; V_{s30}; Quaternary

1. Introduction

The Wasatch Front (**Figure 1**) [1], which is home to over 80% of Utah's population, lies in the hanging wall of the Wasatch Fault Zone (WFZ)—a major normal fault system that forms part of the Intermountain Seismic Belt (ISB), stretching from Montana to Arizona [2]. The fault is segmented, with each segment possessing its own geological history and earthquake potential [3]. One segment can rupture independently or possibly in conjunction with adjacent segments. Additionally, this suggests that the influence of elastic parameters in the shallow subsurface can differ between segments, making site-specific studies essential. The WFZ has been relatively quiet in recent times; however, paleoseismic studies show that large earthquakes (magnitude 6.5–7.5) have occurred repeatedly over the past 10 ka [4]. On average, a significant quake occurs every 300 to 400 years on one of the fault segments, although none have ruptured since European settlement began in the 1800s [4–6]. For any individual segment of the central part of the WFZ, the average recurrence interval is approximately 1.2 to 2.6 thousand years [6]. Seismic risk is rising in the Provo segment (**Figure 1**) as the population increases in this area, which lies in the hanging wall

¹ Coastal and Hydraulics Laboratory, U.S. Army Corps of Engineers Engineer Research and Development Center, Vicksburg, MS 39180, USA

² Department of Geological Sciences, Brigham Young University, Provo, UT 84602, USA

³ Department of Geology and Geophysics, University of Utah, Salt Lake City, UT 84112, USA

^{*} Correspondence: john_mcbride@byu.edu

of the fault zone. The length of the Provo segment is about 70 km when measured along its surface trace [3]. The last major earthquake on this segment is believed to have occurred approximately 500–550 years ago [7]. Since this time, at least 1 m of potential slip has accumulated along the Provo segment of the Wasatch Fault, which could produce at least a moment magnitude 7.0 earthquake.

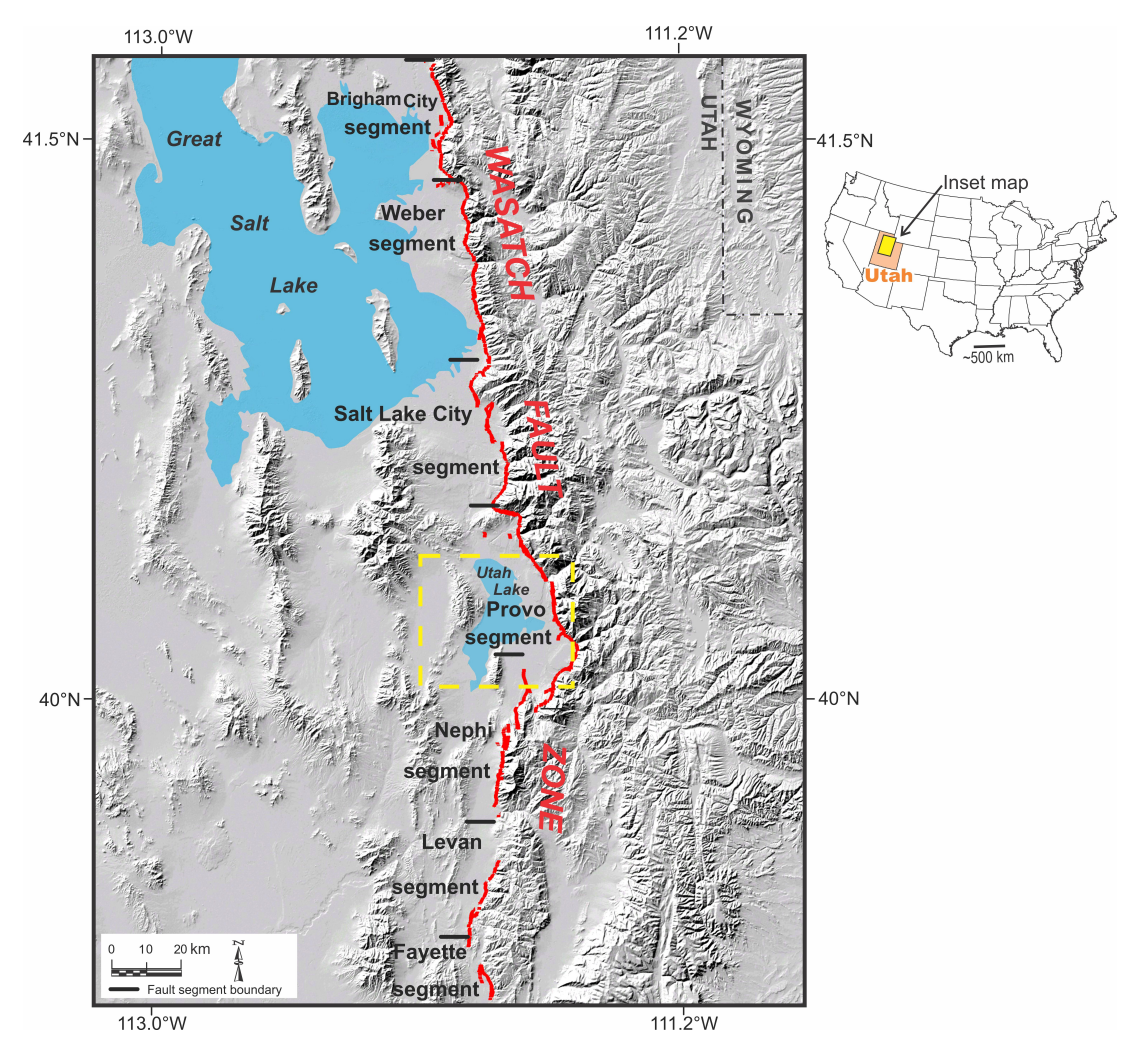


Figure 1. Wasatch Front Urban Corridor with the Wasatch Fault Zone mapped. Fault data from U.S. Geological Survey and Utah Geological Survey [8]. Digital shaded relief data from NASA Shuttle Radar Topography Mission (SRTM) [9]. The dashed yellow outline indicates the study area (see **Figure 2**).

As the population along the WFZ grows, so does the awareness of seismic risk, emphasizing the ongoing need to quickly obtain V_{s30} measurements, especially as open areas suitable for array-based measurements become increasingly scarce. Over the past 30 years, significant progress has been made in developing transformations between V_{s30} and f_0 [10]. This relationship is likely to be most dependable in regions with consistent elastic and geological properties in the shallow subsurface (\leq 30 m). Creating such a transformation for the Provo segment (**Figure 2**) of the WFZ would lessen reliance on more expensive and time-consuming seismic array methods, which face rapidly declining land access.

This study is the first to use HVSR analysis to compare f_0 with V_{s30} for the Provo segment of the WFZ; however, several studies in the study area have measured V_s (shear-wave velocity) variation with depth. McDonald and Ashland [11] compiled results for earthquake site conditions along Wasatch Front urban corridor (**Figure 1**). Earthquake site-response was evaluated with shear wave velocity profiling by Bay [12]. Active-source high-resolution seismic imaging integrated with V_{s30} estimates [13] furnished further constraints for earthquake hazards. A com-

bination of high-resolution seismic imaging and HVSR analysis was used to map shallow bedrock shelves along the hanging wall of the WFZ [14]. Studies comparing V_{s30} and f_0 have been published for other areas worldwide, including populated areas in Alaska [15] and earthquake zones in the eastern USA [16,17]. One of the most comprehensive studies correlating V_{s30} and f_0 in Asia was performed by Kuo et al. [18]. The results of these studies are discussed in greater detail below.

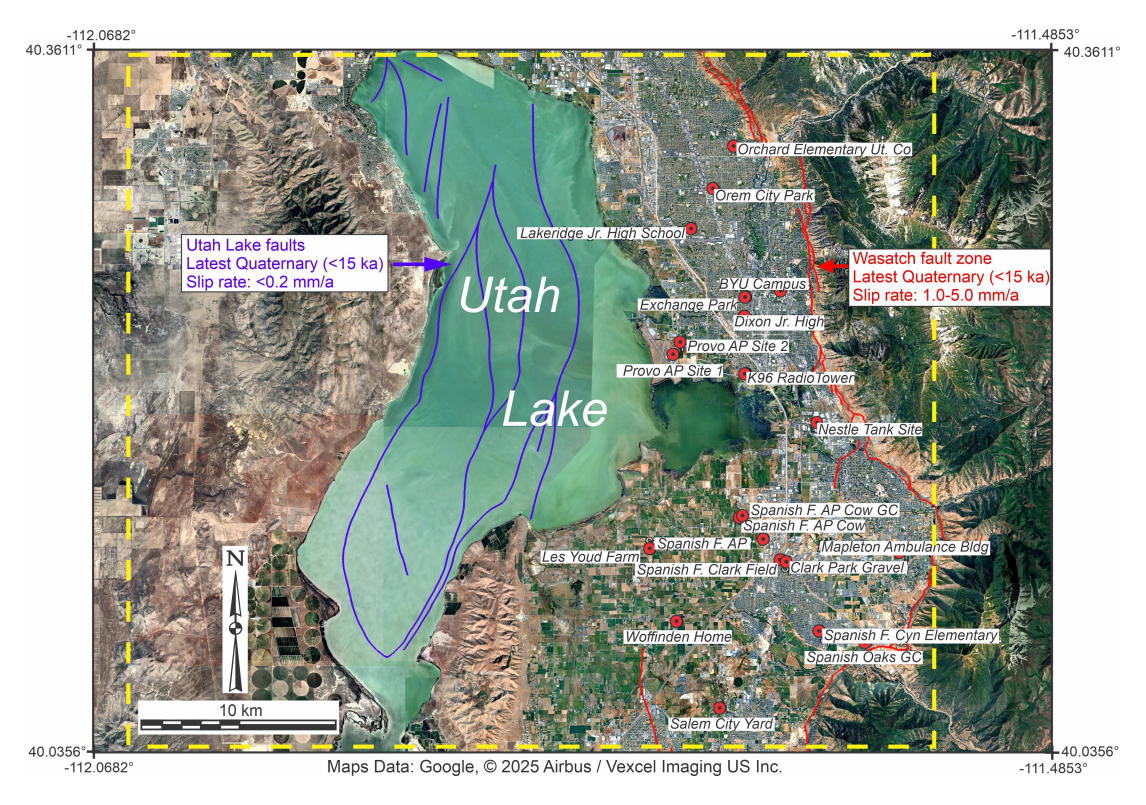


Figure 2. Satellite image of the study area (Provo segment of the Wasatch fault zone, marked with red lines) showing 20 V_{s30} sites surveyed for f_0 using HVSR. Site names match those in the table. The yellow outline corresponds to the outline in **Figure 1**. The fault data sources are the Working Group on Utah Earthquake Probabilities [1] and U.S. Geological Survey and Utah Geological Survey [8].

The objectives of this study are (1) to present the results of seismic surveys for HVSR (horizontal-to-vertical spectral ratio) transformations, aiming to determine the resonant frequency (f_0) for the subsurface in an urbanising area of the hanging wall of the WFZ in northern Utah, USA (the Provo earthquake segment, **Figure 2**); (2) to evaluate any potential for a correlation between the average shear-wave velocity in the upper 30 metres of the subsurface (V_{s30}) and f_0 ; (3) to review the results with respect to previous shear wave velocity (V_s) measurements in the study area, as well as within the broader context of analogous studies in other earthquake zones; (4) to, based on the experimental findings, assess the value of future HVSR work along the ISB to estimate seismic hazard more effectively.

2. Technique

2.1. HVSR Method

The Horizontal-to-Vertical Spectral Ratio (HVSR) method, also known as the Nakamura method, is frequently employed in site investigations to estimate the resonant frequency of soft sediment layers above hard bedrock (e.g., depth < 50 m) [10,19–24]. This approach depends on the ratio of the amplitude spectrum of horizontal ground motion components (H) to the vertical component (V). Peaks on the HVSR curve typically identify resonant frequencies where soft sediments amplify ambient vibrations caused by wind, ocean waves, traffic, or footsteps [23–26]; however, HVSR peaks are not always evident—such as in locations with low acoustic impedance contrast or com-

plex subsurface structures [26,27]. Natural vibrations generally occur within a low-frequency range (e.g., < 1 Hz), whereas human-made or very shallow sources tend to generate higher-frequency components (e.g., > 1 Hz). The technique utilises a small, three-component seismometer to measure passive ground vibrations, making it adaptable to nearly any location [28]. The HVSR method has been utilised to derive site shear-wave velocity (V_s) profiles for engineering purposes, including the evaluation of ground shaking amplification [29–31]. It has also been used to characterise sedimentary cover and determine the depth to underlying bedrock [32–37].

2.2. V_{s30} and Resonant Frequency

 V_{s30} is the main parameter used for classifying a building site for strength and stability [29,37–39]. V_{s30} can be estimated from shear-wave profiles obtained through acoustic borehole logging or surface seismic surveys. The latter includes Spectral Analysis of Surface Waves (SASW) and Multi-channel Analysis of Surface Waves (MASW), which have become standard non-invasive methods for determining V_{s30} [40–42]. HVSR measurements for f_0 are obtained with a single portable, low-frequency, three-component seismometer, recording for as little as 20 minutes [28]. The resonant frequency is sometimes regarded as an alternative to V_{s30} for classifying sites [43–59]; however, it is important to note that V_{s30} characterises layers in the uppermost 30 m, whereas f_0 relates to the layers down to the bedrock or a significant rigidity discontinuity, whose thickness may exceed 30 m. Using f_0 associated with a soft layer with a thickness less than 30 m as a proxy for V_{s30} is not reliable—in such cases, a predicted V_{s30} would be overestimated.

3. Study Area

3.1. Local Sedimentary Geology Setting

The study area in Utah Valley (Figures 2 and 3), northern Utah, is bordered by the Wasatch Range to the east and the Lake Mountains to the west [60]. Utah Valley lies within a fault-bounded half-graben, which forms part of the eastern Basin and Range province, and is filled with unconsolidated to semi-consolidated sediments that are generally up to 1 km or more thick [61,62]. The primary underlying bedrock units mostly consist of carbonate and clastic sedimentary rocks, shales, and sandstones dating from Neoproterozoic to Tertiary [63]. The study mainly concentrates on Quaternary and Tertiary sedimentary units that cover the bedrock (Figure 3). Much of the valley floor, particularly near Utah Lake, is covered by sediments from Pleistocene Lake Bonneville and alluvial deposits originating from the mountains to the east and west [64,65]. Beach and deltaic sediments associated with ancient Lake Bonneville include gravel, sand, and silt deposits. Lacustrine sediments, made up of fine-grained silt, clay, and marl, were deposited in the deeper, calmer parts of the lake [64,65]. The thickness of Lake Bonneville deposits in Utah Valley varies greatly depending on the sedimentary environment. Research by the Utah Geological Survey, the U.S. Geological Survey, and others [66,67] suggests an average thickness of 15 to 45 m for shoreline lacustrine sediments and deltaic deposits, and 3 to 15 m for deposits from deeper water. Alluvial deposits typically consist of poorly to moderately sorted layers of gravel, sand, silt, and clay. In central and western Utah Valley, alluvial deposits can be over 60 m thick in certain areas, especially near the mountain range in current or ancient stream drainage [66,67].

3.2. Local Seismic Hazard Setting

The WFZ [64] dominates seismic hazard in Utah Valley and nearby areas along the ISB. Seismic hazard assessment for the Utah Valley west of the WFZ has been carried out at specific test sites using seismic surveys (e.g., MASW, SASW) or borehole logging [11–14,61]. Key studies include: seismic shear (S) wave velocity testing led by the U. S. Geological Survey with a Minivib energy source, which reported V_{s30} values of 160–690 m/s, corresponding to NEHRP site classifications of C to E [68,69]; collection and analysis of V_{s30} data by the Utah Geological Survey for several locations along the Wasatch Front urban corridor, mainly classified as D according to the IBC (International Building Code) (V_s = 174–300 m/s) [69]; a report on V_{s30} values in urban regions along the Wasatch Front using SASW [11]; and an integrated S-wave and P-wave seismic transect in southern Utah Val-ley, which identified S-wave velocities of approximately 200 m/s at the surface rising to about 900 m/s at 160 m depth [61]. The U. S. Geological Survey NEHRP seismic hazard map for Utah Valley and surrounding areas [68] presents a probability range (2% in 50 years) of ground acceleration from 20 to 80 (% g).

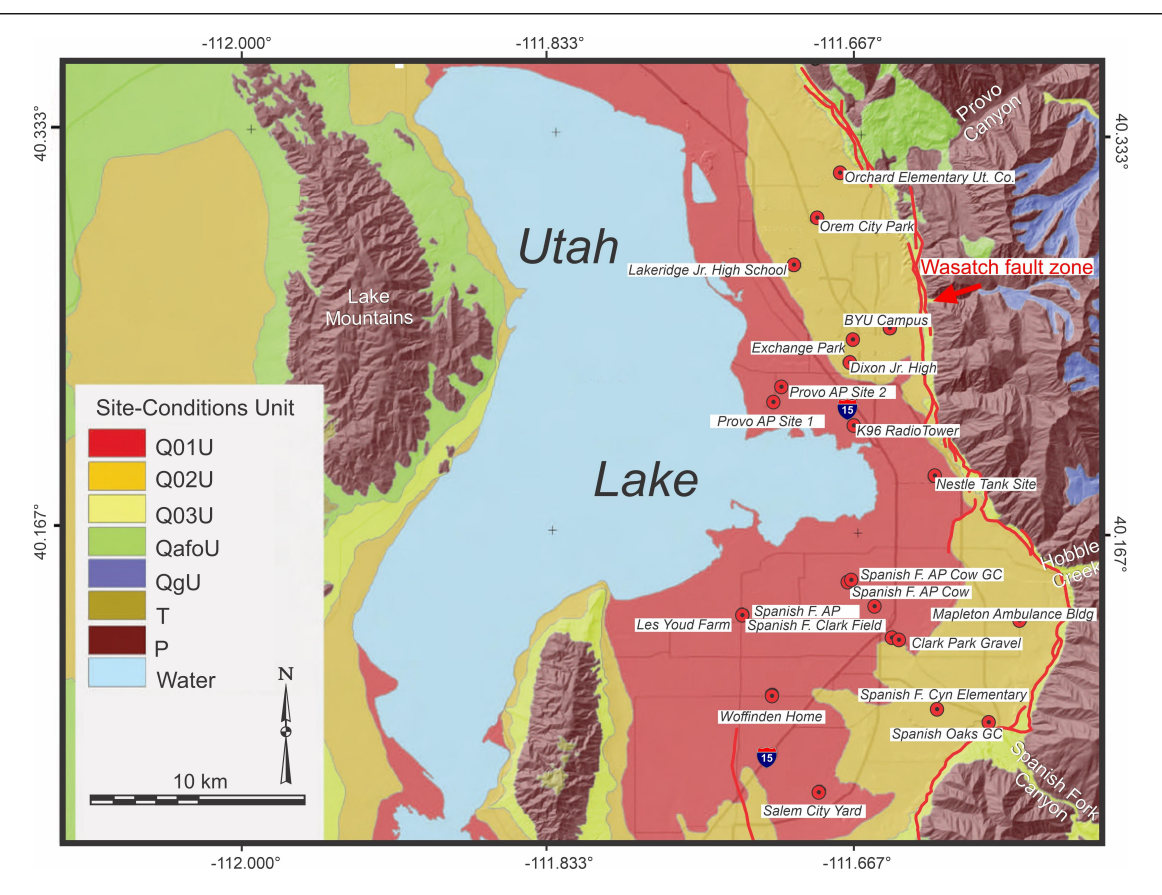


Figure 3. Site conditions map for the study area (**Figure 2**), modified with permission from the Utah Geological Survey [11]. Q01U: Lacustrine and alluvial silt, clay, and fine sand. Q02U: Lacustrine sand and gravel, latest Pleistocene to Holocene alluvial-fan deposits. Q03U: Lacustrine and alluvial gravel and sand, pre-Bonneville alluvial-fan deposits. QafoU: Pre-Bonneville alluvial-fan gravel, sand, silt, and cobbles. Qg: Glacial deposits. T: Tertiary bedrock. P: Palaeozoic and Precambrian bedrock.

4. Methods

The procedure began with revisiting sites previously surveyed for V_{s30} by the U. S. Geological Survey and the Utah Geological Survey in Utah County, Utah [11–13]. The f_0 was derived using HVSR with a three-component TROMINO® seismometer (minimum 0.1 Hz). The seismometer operated at a sampling rate of 128 Hz, enabling the identification of amplification peaks up to 64 Hz (the Nyquist frequency). It was oriented northward, coupled to firm ground with spikes, levelled, and set to record for 30 minutes (**Figure 4**). In all cases, the ground was wet or moist during the HVSR survey. Rainfall for the November and December 2023 survey period (for Provo, Utah and vicinity) was respectively 4.60 and 2.06 cm [70]. Averages for those two months are respectively 3.53 cm and 4.60 cm for 1991–2020 or a cumulative value of only 1.47 cm greater than for the survey period [70] and thus not unusual for the study area. Increasing moisture content can initially increase the V_s due to capillary forces although this effect would only apply to the upper few centimetres of the soil zone [71].

Amplitude-frequency spectra were calculated for the three components (N-S, E-W "H", and up-down "V"), then converted to the H/V response as a function of frequency using the GRILLATM modelling software [26,28]. The f_0 was identified by selecting the highest H/V spectral peak. Noisy segments of the 30-minute recordings were carefully edited where necessary, based on cluttered frequencies, to reduce uncertainty in the time-frequency transformation. The f_0 ranged from 0.28 to 1.38 Hz at all sites except two, which exhibited anomalously high frequency responses (> 40 Hz). Each site was classified according to the IBC (International Building Code) or NEHRP [69] building code, as well as the Quaternary site conditions unit (**Table 1**). After HVSR analysis, the sites were graded (A+ to F) based on the quality of the f_0 peak, noise levels, and the uncertainties in f_0 and H/V. Measurements were discarded if the f_0 uncertainty [26,28] exceeded \pm 0.5 or if the H/V uncertainty was greater than \pm 1. As discussed above, it is crucial

to use only sites where the soft layer (i.e., above and excluding rigid bedrock) exceeds 30 m in thickness. Based on the V_{s30} measurements by McDonald and Ashland [11], Bay [12], and Stephenson et al. [13], the shallow V_s layer thickness at all sites exceeded 30 m (**Figure 5**), using the criterion of $V_s \ge 400$ m/s for rigid bedrock, as derived by Nelson and McBride [14]. Additionally, the selection of sites was limited to a relatively narrow north-south corridor, approximately 15 km wide (**Figure 3**), to minimise significant variations in shallow-layer thickness west of the WFZ. The V_s function compilation (**Figure 5**) shows some low-velocity fluctuation in the upper 15 m. For example, the DPA function (**Figure 5**) was accompanied by a borehole lithology log that showed a change from "very soft clay" to "an increase in sand content", respectively manifested by a jump in V_s from 130 m/s to 185 m/s [13]. Detailed information about the individual sites is given in **Table 1**.



Figure 4. Photo showing the levelling of the seismometer and orienting it north at the "Spanish Oaks GC" field site (**Figure 2** and **Table 1**).

Table 1. Parameter listing for all 20 V_{s30} sites surveyed with the three-component seismometer for which HVSR analysis was performed.

Site	Lat.	Long. (-)	Unit	V _{s30} (m/s)	f ₀ (Hz)	f ₀ Uncertainty (Hz)	H/V Uncertainty (Hz)	Peak Quality	Grade	V _{s30} Source
Nestle Tank	40.1891	111.6250	Q01U	162	0.88	± 0.07	± 0.3489	A	A+	McDonald and Ashland [11]
Orem Park	40.2966	111.6910	Q03U	323	1.13	± 0.03	± 0.6142	C	A	McDonald and Ashland [11]
Provo Ap 1 (DPA)	40.2230	111.7210	Q01U	161	0.91	± 0.04	± 0.5605	С	В	Stephenson et al. [13]
Les Youd (LSU)	40.1306	111.7290	Q01U	169	0.28	± 0.05	± 0.6871	С	A-	Bay [12]
*Span. F. Cyn Element. (SFCE)	40.0928	111.6261	Q02U	350	0.69	± 0.05	± 1.1305	F	С	Stephenson et al. [13]
Span. F. Clark (SFCP)	40.1258	111.6501	Q01U	230	1.19	± 0.06	± 0.3780	A	В	Stephenson et al. [13]
Mapleton Ambulance (MAB)	40.1294	111.5780	Q02U	266	1.25	± 0.07	± 0.4469	В	A	Bay [12]
Provo AP 2 (PA)	40.2265	111.7109	Q01U	160	0.91	± 0.08	± 0.6391	С	A	Stephenson et al. [13]
BYU Campus (BYU)	40.2508	111.6500	Q02U	256	0.88	± 0.10	± 0.4403	В	A	Bay [12]
K96 radio (K96)	40.2120	111.6710	Q01U	202	0.88	± 0.11	± 0.3103	A	A	Stephenson et al. [13]
Orchard Element. (OES)	40.3173	111.6781	Q03U	341	1.38	± 0.11	± 0.4974	В	A-	Bay [12]
*Woffinden (WOF)	40.0972	111.7130	Q01U	157	0.53	± 0.12	± 1.2911	F	F	Bay [12]
Span. F. AP (DSFA)	40.1350	111.6610	Q01U	223	0.94	± 0.18	± 0.3993	A	A	Stephenson et al. [13]
Span. F. AP Cow (SFA)	40.1452	111.6737	Q01U	200	0.91	± 0.21	± 0.3180	A	A	Stephenson et al. [13]
Salem Yard (SCY)	40.0567	111.6870	Q01U	175	0.94	± 0.23	± 0.4818	В	A-	Bay [12]
Exchange Park (ÉP)	40.2475	111.6711	Q02U	190	1.09	± 0.33	± 0.4919	В	A-	Stephenson et al. [13]
Lakeridge JH (LRJ)	40.2768	111.7030	Q02U	232	1.09	± 0.36	± 0.5688	C	В	Bay [12]
*Dixon JH (DJH)	40.2366	111.6720	Q02U	211	1.13	± 0.69	± 0.4125	В	A	Bay [12]
*Clark Park G. (SFCP)	40.1249	111.6468	Q01U	230	54.06	± 0.97	± 1.2218	F	С	Stephenson et al. [13]
*Spanish Oaks (SOGC)	40.0877	111.5984	Q03U	370	41.25	± 4.27	± 0.2340	A	A+	Stephenson et al. [13]

Note: Entries marked with an asterisk indicate measurements with quality insufficient for analysis. Abbreviations in Site column correspond to V_s profiles in **Figure 5**.

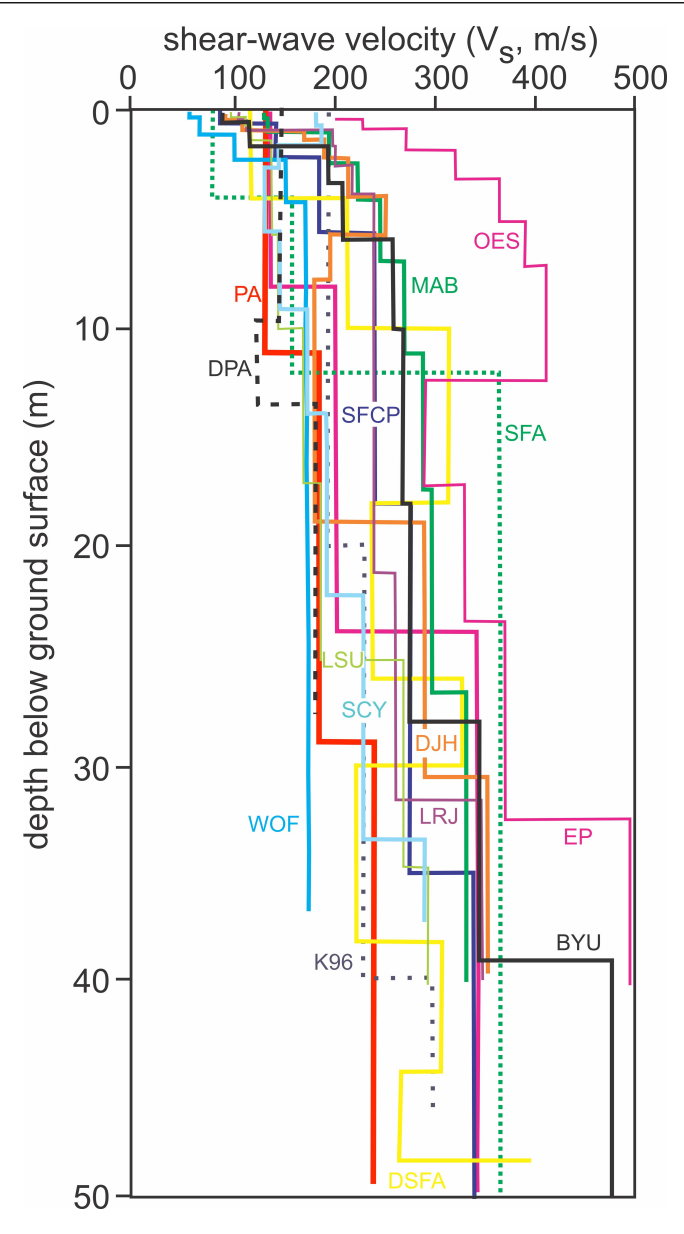


Figure 5. One-dimensional shear-wave velocity profiles from McDonald and Ashland [11], Bay [12], and Stephenson et al. [13], from which V_{s30} was derived (see **Table 1**). Labels correspond to those used by Bay [12] and Stephenson et al. [13].

5. Results

Table 1 presents the 20 sites surveyed in Utah Valley, including their locations, site condition units within the Quaternary Period, V_{s30} , f_0 , uncertainties, interpreted quality factors, and data sources. Fifteen of these measurements met the acceptance criteria for minimal uncertainty, as described in the Methods section above, and were included in the analysis. The results from these sites can be considered a coherent group because (1) the study area is limited to a single segment of the WFZ, specifically the Provo segment (recall that these segments are defined by their earthquake phenomenology, such as recurrence interval and slip rate); (2) the lithology of materials in the upper 30 m is generally consistent—unconsolidated to semi-consolidated Quaternary sands, gravels, and finer-grained sediments—with a pre-determined NEHRP site classification of primarily C-D; (3) the underlying bedrock is expected to be fairly uniform in terms of elastic parameters, mostly Palaeozoic carbonate and clastic sedimentary rocks [66]; (4) all sites are located within the hanging wall of the WFZ, confined to a narrow 30 km long north-south corridor, approximately 15 km wide, between the WFZ and the eastern shores of Utah Lake (**Figure**

2); (5) the fieldwork was conducted over a short, approximately one-month period, in November-December 2023. Representative examples of the H/V inversions are shown for Site-Condition Quaternary Units Q01U, Q02U, and Q03U (NEHRP site classifications D and E) (**Figure 6**). For each example, speed is plotted as a function of frequency for the three components, the H/V ratio is plotted as a function of frequency, and the histogram of frequency amplitude over recording time is displayed. The latter was used to identify and exclude noisy periods. Most spectra feature a narrow high-frequency peak between 11 and 13 Hz, likely indicating a shallow soil layer. The thickness of this shallow layer overlying bedrock can be estimated using the fundamental mode equation [37–39]. For instance, at the Nestle Tank site (**Table 1**), with a pre-determined V_{s30} of 162 m/s and a high-frequency peak at 12 Hz, the shallow layer would be approximately 3.4 m thick. Frequencies like these do not correspond to the interpreted f₀ value. The strongest low-frequency peak on the spectra, identified as f₀, ranged from 0.28 to 1.38 Hz (**Figure 6**). The character of the low-frequency portion of the spectra (< 2 Hz) varies from a well-defined peak (e.g., Lakeridge Jr. High, **Figure 6**) to more complicated with more than one peak (Salem City Yard, **Figure 6**).

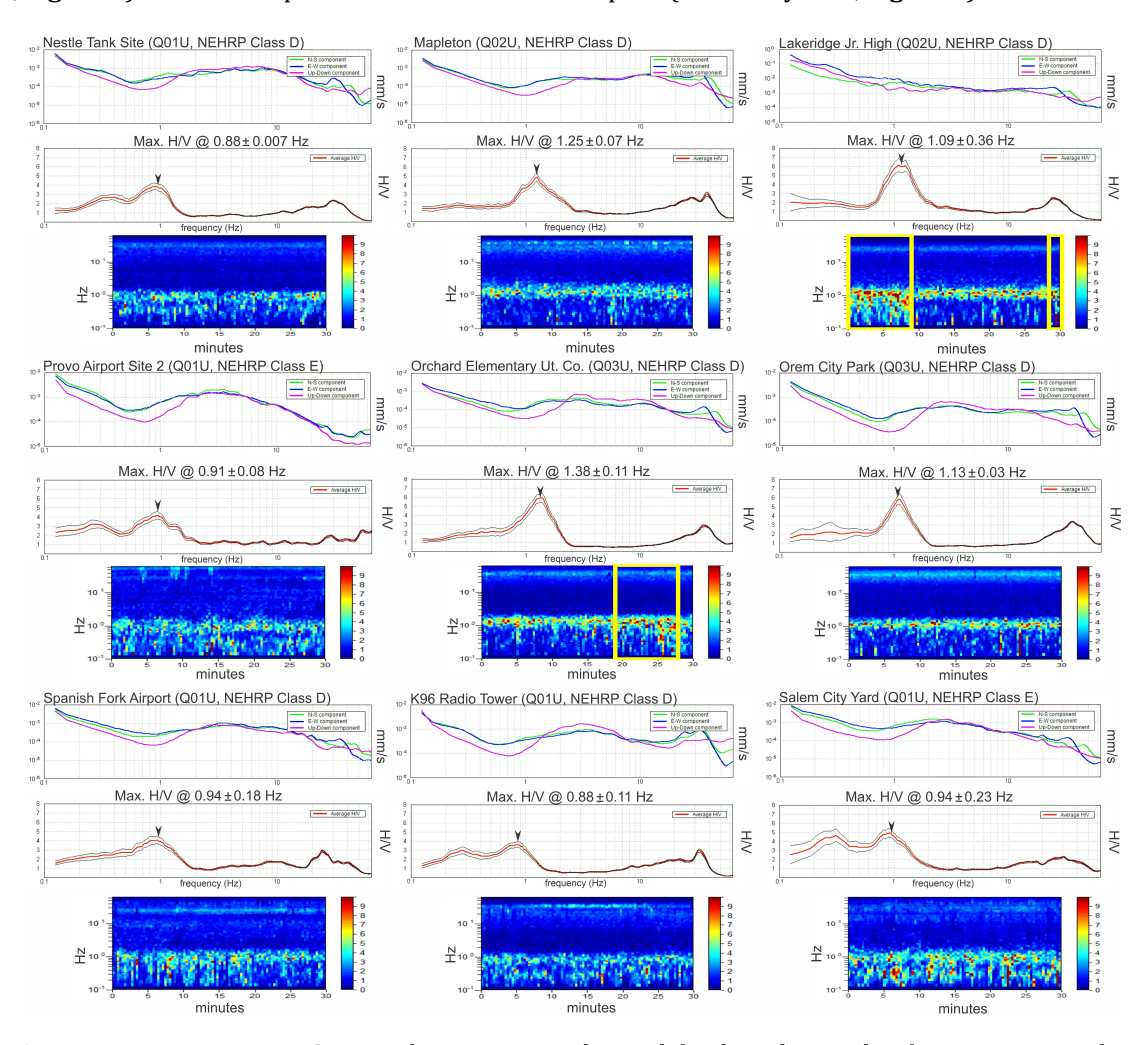


Figure 6. Nine representative HVSR transformations. Each panel displays the amplitude response as a function of frequency for the three components (top), the H/V ratio as a function of frequencies (middle), and the histogram of frequency amplitude over recording time (bottom). Especially noisy sections were muted (yellow rectangles) as needed.

To enhance understanding of the HVSR transformation (**Figure 6**), from which f_0 was derived, forward modelling was performed of the H/V spectra (**Figure 7a**). Forward modelling (**Figure 7b**) was performed using the GrillaTM software package [28] to inspect for deeper boundaries, likely between bedrock ($V_s > 400 \text{ m/s}$) and the overlying Quaternary valley fill. In all cases, the V_s of bedrock layers was adjusted to match the resonant peak (f_0)

amplitude, and the depth to bedrock varied to match the frequency of f_0 . Where available, estimates of Poisson's ratio and bulk density for Quaternary sediments [12] were incorporated into the modelling. Six sites reported by Bay [12] provided estimates of Poisson's ratio (0.45) and bulk density (1.9 g/ml) for Quaternary sediments, and respectively 0.3 and 2.6 g/ml for bedrock.

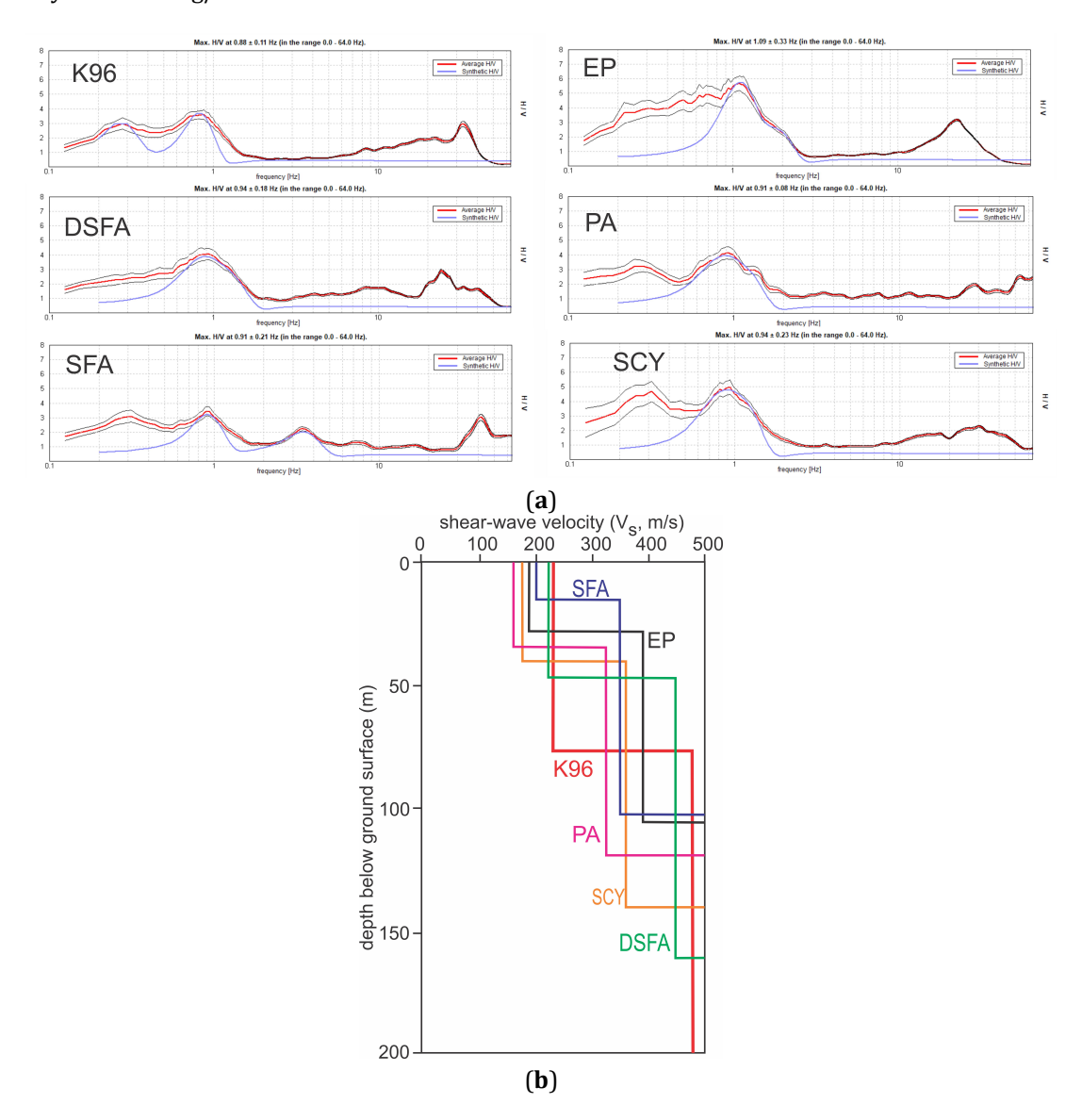


Figure 7. (a) Representative examples of the forward modelling that matched the frequency and amplitude of the HVSR resonant frequency (f_0) . The lettered labels refer to sites listed in **Table 1**. The red curve is the average H/V Fourier transformation (**Figure 6**), and the blue curve is the synthetic model curve for the resonant frequency (f_0) ; (b) Representative results of the forward V_s modelling, based on the synthetic H/V transformations shown in **Figure 7a**.

6. Discussion

Previous studies have integrated HVSR f_0 and V_{s30} using linear regression to establish a transformation where the former can be used as a readily obtainable proxy for the latter [43–46]. Experimental linear regression was applied to the 15 high-quality pairs of V_{s30} and f_0 . Ordinary two-dimensional linear regression seeks to model the relationship between the dependent variable (V_{s30} , the "target") and an independent variable (f_0 , the "predictor") by fitting a linear equation ("best-fitting line") to the data [72]. The Multiple R value and p-value were calculated to assess the statistical significance of the correlation [72], and a linear relationship linking f_0 to V_{s30} was derived. The

p-value indicates how well the data support the null hypothesis—that no correlation exists between V_{s30} and f_0 [72]. The result of the regression experiments (Figure 8) showed a Multiple R of 0.6427 (or R-squared = 0.4130) and a pvalue of 0.0098 for the equation $V_{s30} = 148*f_0 + 75$ m/s with a 95% confidence interval. The *p*-value is less than the commonly used significance level of 0.05 [72], suggesting the result is statistically significant. The standard error is 45.3 m/s, and the correlation coefficient is 0.64. Multiple R represents the correlation coefficient between observed and predicted values of the dependent variable (here, V_{s30}), ranging from 0 to 1, with values closer to 1 indicating a strong linear relationship [72]. A Multiple R of 0.4130 indicates that the transformation can only explain 41.3% of the variation in V_{s30} —the remaining 58.7% of the variance remains unexplained, suggesting that other factors not included in the analysis also influence the outcome and that the transformation's predictive power is limited. The unexplained residual behaviour (**Figure 8**) could be related to the small sample size (15) or to missing predictors. The latter may include the assumption that bedrock lies not too deeply below 30 metres in the previously measured shear-wave velocity profiles (Figure 5). As mentioned above, sites were avoided where the thickness of the soft layer within the $V_{\rm s30}$ interval (defined as < 400 m/s, discussed above) is less than 30 metres. In this way, a shallow, harder bedrock is less likely to bias $V_{\rm s30}$ and thus influence a linear transformation. On the other hand, a bedrock depth significantly greater than 30 metres could also compromise the meaning of the transformation. For example, Stephenson and Odum [73] demonstrated that a deeply buried (e.g., 300 m) base of unconsolidated sediments in the Salt Lake Valley of Utah (Figure 1) can induce resonance in the 1-3 Hz range. Therefore, it is possible that part of the H/V response in the low- f_0 range could result from a much deeper bedrock (i.e., with $V_s > 400$ m/s).

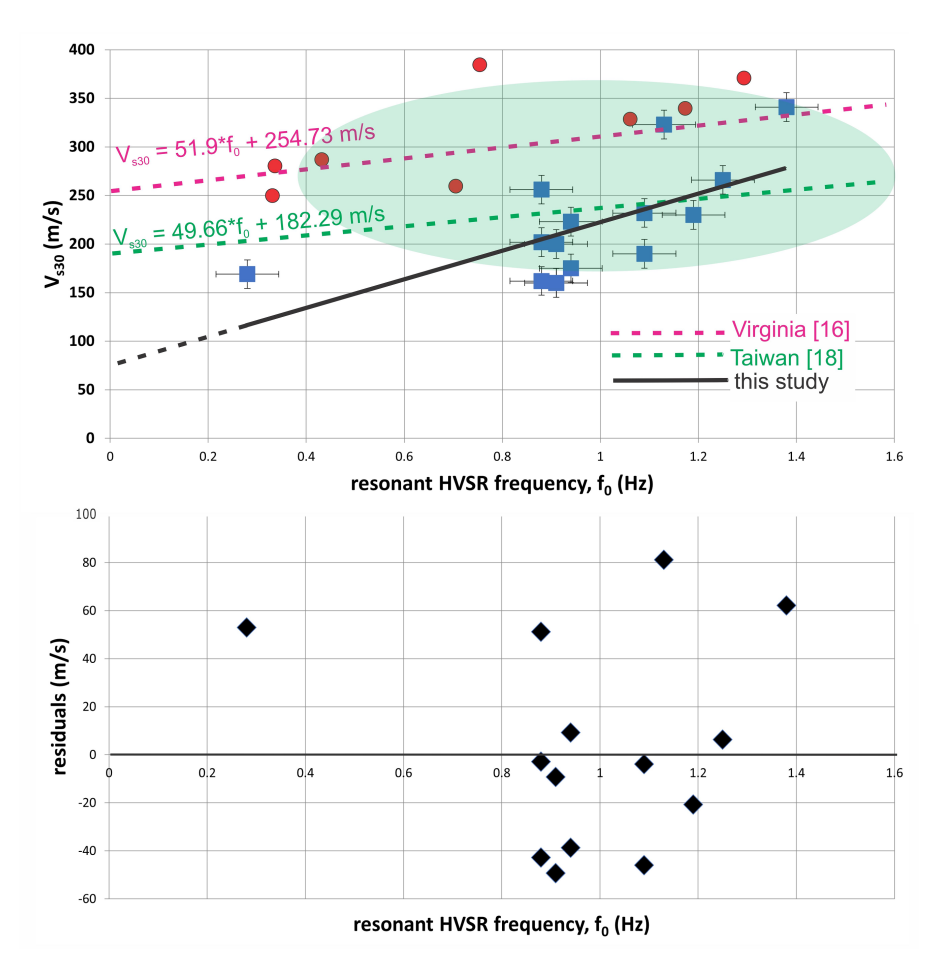


Figure 8. Top, results of linear regression for this study (Provo segment of WFZ) (blue squares with standard error shown) compared with two analogous studies. Red dots represent data points extracted from McNamara et al. [16]. The green-shaded envelope represents the region of several data points from Kuo et al. [18]. Bottom, residual plot for the regression.

From the plot in **Figure 8**, it is clear that including more V_{s30} - f_0 pairs for low shear-wave velocities (i.e., 0.3 Hz < f_0 < 0.9 Hz) is necessary to fully constrain the regression for the weakest ground sites, specifically NEHRP class E. Such sites may be overlooked or excluded from studies intended to provide practical guidance for development [74–76]. For example, studies in the Sacramento-San Joaquin Delta, near San Francisco, California, where the upper 30 m of the subsurface comprises levee fill and peat layers, have yielded very low V_{s30} values (62.2–200.1 m/s) and minimum values of 35 m/s [74,75]. For the lowest f_0 from the experimental linear regression (**Figure 8**), one would expect V_{s30} values of approximately 75 m/s, like those observed in the Sacramento-San Joaquin Delta [74]. Presumably, such values could be found in wetland and marshy areas along the unpopulated southeastern shores of Utah Lake (**Figures 2** and **3**).

The values for V_{s30} and f₀ for the Provo segment can be compared to similar studies from different geological environments. For example, Thornley et al. [15] identified a positive logarithmic correlation between V_{s30} and f_0 for an area near Anchorage, Alaska (USA), with V_{s30} values ranging from about 100 m/s to 600 m/s and peak frequencies approximately between 1 and 6 Hz. The soil sites included dense glacial till and lacustrine sediments. A detailed V_s velocity study in southwestern Taiwan, utilizing the Engineering Geological Database from the Taiwan Strong Motion Instrumentation Programme [18], produced a linear regression equation of $V_{s30} = 49.66 * f_0 + 182.29$ with a 95% confidence interval (Figure 8). The geological units were mainly Quaternary formations classified under NEHRP site classes D-B, which are significantly stiffer (higher V_{s30}) than those in the Utah study area. Many of the dominant frequencies reported in the Taiwan study were considerably higher, as expected for stiffer materials. The lowest V_{s30} f_0 pairs overlapped the data in part (Figure 8). One of the most comprehensive studies examining V_{s30} and f_0 in the contiguous USA was conducted within the Central Virginia seismic zone, Virginia, USA [77], which experienced the August 2011 Mineral, Virginia, earthquake [16]. Using V_{s30} values and co-located HVSR peak frequencies (interpreted as f_0) for 21 seismograph stations near the earthquake's epicentre, McNamara et al. [16] and Stephenson et al. [17] derived a linear regression equation, $V_{s30} = 51.90*f_0 + 254.73$. This result aligns more closely with that reported for southwestern Taiwan, as mentioned earlier, but still differs significantly from the experimental regression equation for the Provo segment of the WFZ. Like the Taiwan study [18], shallow materials had V_{s30} values between 200 and 900 m/s, and HVSR peak frequencies ranged from approximately 0.1 to 10 Hz. Again, both parameters exceed those observed at the Quaternary sites within the Provo segment. Additionally, their regression line lies above most of the Utah data points (Figure 8). The wide variation in subsurface materials in the Virginia study area, which included solid rock as well as highly weathered and saturated soils, explains this difference. Furthermore, their NEHRP site classes were higher, B-D.

Forward shear-wave velocity-depth modelling (**Figure 7b**) from the HVSR spectra (**Figure 7a**) indicates that the shallow subsurface (< 30 m) for the sites has a $V_s < 400$ m/s, which helps to satisfy the requirement that the depth zone over which V_{s30} is measured is not influenced by the higher- V_s "seismic" bedrock below. Since the HVSR-derived V_s models are based on the recording of low-frequency ambient noise, less complexity is expected in the models (**Figure 7b**), relative to models based on MASW, SASW, or downhole velocity modelling (**Figure 5**).

7. Conclusions

As population density rises along the Wasatch Fault Corridor Utah (USA), seismic risk also increases. V_{s30} is required to evaluate potential shaking due to an earthquake but can be challenging to obtain. The resonant frequency of a ground site (f_0) may be an easily measured proxy for V_{s30} . Twenty sites with pre-established high-quality V_{s30} measurements were re-occupied using a 30-minute recording with a three-component seismometer to compute the HVSR of the Fourier amplitude spectra and derive f_0 . A quality-control rubric identified 15 of the HVSR results as suitable for analysis. This study is novel as the first of its kind along the Wasatch Fault Zone (WFZ). The robustness of the study could be enhanced with additional data points. The number of data points (15) is comparable to those used in the cited studies of the Central Virginia seismic zone. For accepted sites, f_0 values ranged from 0.28 to 1.38 Hz, with V_{s30} values of 162 to 341 m/s. The associated NEHRP site classes ranged from C to E ("very dense soil and soft rock" to "soft clay soil"). This study demonstrates potential for expanding more coincident V_{s30} and HVSR measurements along the WFZ. Although the linear transformation derived can be considered statistically significant, its predictive power could potentially be improved with more measurements. More coincident HVSR and

 V_{s30} surveys would be useful, especially for frequencies below about 0.8 Hz. The findings are promising for utilising f_0 HVSR measurements to rapidly estimate V_{s30} along the Provo segment of the WFZ. Future work following this procedure should extend to other parts of the WFZ, particularly in areas experiencing increasing population and infrastructure development.

Author Contributions

Conceptualization, J.M., R.A.H. and S.T.N.; methodology, J.M., K.J.S., K.A.R. and B.W.; software, J.M., K.J.S., S.T.N. and B.W.; formal analysis, K.J.S. and J.M.; investigation, J.M., K.J.S., B.W. and K.A.R.; data curation, K.J.S. and J.M.; writing—original draft preparation, J.M. and K.J.S.; writing—review and editing, J.M. and K.J.S.; visualization, J.M. and K.J.S.; supervision, J.M. and R.A.H.; project administration, J.M. and R.A.H.; funding acquisition, R.A.H. All authors have read and agreed to the published version of the manuscript.

Funding

The College of Physical and Mathematical Sciences at Brigham Young University funded this project.

Institutional Review Board Statement

Not applicable.

Informed Consent Statement

Not applicable.

Data Availability Statement

The data sets presented in this article are not readily available because the data are part of an ongoing study.

Acknowledgments

The authors express appreciation to W. J. Stephenson and A. P. McKean and two anonymous referees for their comments and recommendations, which substantially improved the article.

Conflicts of Interest

The authors declare no conflicts of interest. The funders had no role in the design of the study; in the collection, analyses, or interpretation of data; in the writing of the manuscript; or in the decision to publish the results.

References

- 1. Working Group on Utah Earthquake Probabilities (WGUEP). *Earthquake probabilities for the Wasatch Front region in Utah, Idaho, and Wyoming*; Utah Geological Survey: Salt Lake City, UT, USA, 2016; pp. 3–21.
- 2. Smith, R.B.; Arabasz, W.J. Seismicity of the Intermountain Seismic Belt. In *Neotectonics of North America*; Slemmons, D.B., Engdahl, E.R., Zoback, M.D., et al., Eds.; Geological Society of America: Denver, CO, USA, 1991; pp. 185–228.
- 3. Machette, M.N.; Personius, S.F.; Nelson, A.R. The Wasatch fault zone, Utah—segmentation and history of Holocene earthquakes. *J. Struct. Geol.* **1991**, *13*, 137–149. [CrossRef]
- 4. McCalpin, J.P. Application of paleoseismic data to seismic hazard assessment and neotectonic research. *Internat. Geophys.* **1996**, *62*, 439–493. [CrossRef]
- 5. McCalpin, J.P.; Nishenko, S.P. Holocene paleoseismicity, temporal clustering, and probabilities of future large (M > 7) earthquakes on the Wasatch fault zone, Utah. *J. Geophys. Res.* **1996**, *101*, 6233–6253. [CrossRef]
- 6. Utah Geological Survey. *The Wasatch Fault. Public Information Series 40*; Utah Geological Survey: Salt Lake City, UT, USA, 1996; pp. 3–15.
- 7. Toké, N.A.; Phillips, J.; Langevin, C.; et al. The Traverse Ridge Paleoseismic Site and Ruptures Crossing the Boundary Between the Provo and Salt Lake City Segments of the Wasatch Fault Zone, Utah, United States. *Front. Earth Sci.* **2021**, *9*, 607018. [CrossRef]

- 8. U.S. Geological Survey; Utah Geological Survey. Quaternary fault and fold database for the United States. Available online: https://www.usgs.gov/natural-hazards/earthquake-hazards/faults (accessed on 4 July 2025).
- 9. NASA Shuttle Radar Topography Mission (SRTM). Shuttle Radar Topography Mission (SRTM) Global. Available online: https://doi.org/10.5069/G9445JDF (accessed on 25 August 2025).
- 10. Hassani, B.; Atkinson, G.M. Applicability of the Site Fundamental Frequency as a VS30 Proxy for Central and Eastern North America. *Bull. Seismol. Soc. Am.* **2016**, *106*, 653–664. [CrossRef]
- 11. McDonald, G.N.; Ashland, F.X. Earthquake site conditions in the Wasatch Front urban corridor, Utah. Available online: https://ugspub.nr.utah.gov/publications/special_studies/ss-125.pdf (accessed on 4 July 2025).
- 12. Bay, J.A. Shallow shear wave velocity profiling of poorly characterized earthquake site-response units in urban Utah, Davis, and Weber Counties, Utah. Available online: https://earthquake.usgs.gov/cfusion/external_grants/reports/05HQGR0088.pdf (accessed on 4 July 2025).
- 13. Stephenson, W.J.; Williams, R.A.; Odum, J.K.; et al. Miscellaneous high-resolution seismic imaging investigations in Salt Lake and Utah Valleys for earthquake hazards. In *USGS Open-File Rep 2007–1152*; Geological Survey (U.S.): Reston, VA, USA, 2007. [CrossRef]
- 14. Nelson, S.T.; McBride, J. Seismic mapping of shallow bedrock shelves in the hanging wall of the Wasatch fault. *I. Appl. Geophys.* **2023**, *210*, 1–14. [CrossRef]
- 15. Thornley, J.D.; Dutta, U.; Douglas, J.; et al. Evaluation of horizontal to vertical spectral ratio and standard spectral ratio methods for mapping shear wave velocity across Anchorage, Alaska. *Soil Dyn. Earthq. Eng.* **2021**, *150*, 106918. [CrossRef]
- 16. McNamara, D.E.; Stephenson, W.J.; Odum, J.K.; et al. Site response in the eastern United States: A comparison of Vs30 measurements with estimates from horizontal:vertical spectral ratios. In *The 2011 Mineral, Virginia, Earthquake, and Its Significance for Seismic Hazards in Eastern North America*; Horton Jr., J.W., Chapman, M.C., Green, R.A., Eds.; Geological Society of America: Denver, CO, USA, 2015; pp. 67–79. [CrossRef]
- 17. Stephenson, W.J.; Odum, J.K.; McNamara, D.E.; et al. Ground-motion site effects from multimethod shearwave velocity characterization at 16 seismograph stations deployed for aftershocks of the August 2011 Mineral, Virginia, earthquake. In *The 2011 Mineral, Virginia, Earthquake, and Its Significance for Seismic Hazards in Eastern North America*; Horton Jr., J.W., Chapman, M.C., Green, R.A., Eds.; Geological Society of America: Denver, CO, USA, 2015; pp. 47–65. [CrossRef]
- 18. Kuo, C.-H.; Wen, K.-L.; Lin, C.-H.; et al. Investigating near surface S-wave velocity properties using ambient noise in southwestern Taiwan. *Terr. Atmos. Ocean. Sci.* **2015**, *26*, 205–211. [CrossRef]
- 19. Lim, D.; Ahn, J.-K. Horizontal seismic wave at ground surface from transfer function based on ambient noise. *Front. Earth Sci.* **2023**, *11*, 1047667. [CrossRef]
- 20. Cox, B.R.; Tianjian, C.; Vantassel, J.P.; et al. A statistical representation and frequency-domain window-rejection algorithm for single-station HVSR measurements. *Geophys. J. Int.* **2020**, *221*, 2170–2183. [Cross-Ref]
- 21. Hayashi, K.; Asten, M.W.; Stephenson, W.J.; et al. Microtremor array method using spatial autocorrelation analysis of Rayleigh-wave data. *J. Seismol.* **2022**, *26*, 601–627. [CrossRef]
- 22. Ulysse, S.; Boisson, D.; Prépetit, C.; et al. Site effect assessment of the Gros-Morne Hill area in Port-au-Prince, Haiti, Part A: Geophysical-seismological survey results. *Geosciences* **2018**, *8*, 142. [CrossRef]
- 23. Nakamura, Y. A method for dynamic characteristics estimation of subsurface using microtremor on the ground surface. *Q. Rep. Railway Tech. Res. Inst.* **1989**, *30*, 25–33.
- 24. Nakamura, Y. On the H/V spectrum. In Proceedings of the 12th World Conference on Earthquake Engineering, Beijing, China, 12 October 2008.
- 25. Arai, H.; Tokimatsu, K. S-wave velocity profiling by inversion of microtremor H/V spectrum. *Bull. Seismol. Soc. Am.* **2004**, *94*, 53–63. [CrossRef]
- 26. Castellaro, S. The complementarity of H/V and dispersion curves. *Geophysics* **2016**, *81*, 1–16. [CrossRef]
- 27. Nelson, S.; McBride, J. Application of HVSR to estimating thickness of laterite weathering profiles in basalt. *Earth Surf. Process. Landf.* **2019**, *44*, 1365–1376. [CrossRef]
- 28. Castellaro, S.; Mulargia, F.; Bianconi, L. Passive seismic stratigraphy: a new efficient, fast and economic technique. *Geol. Tecn. Ambientale* **2005**, *3*, 76–102.
- 29. Konno, K.; Ohmachi, T. Ground-motion characteristics estimated from spectral ratio between horizontal and vertical components of microtremor. *Bull. Seismol. Soc. Am.* **1998**, *88*, 228–241. [CrossRef]
- 30. Del Monaco, F.; Tallini, M.; De Rose, C.; et al. HVNSR survey in historical downtown L'Aquila (central Italy):

- site resonance properties vs. subsoil model. Eng. Geol. 2013, 158, 34-47.
- 31. Stanko, D.; Markušić, S.; Strelec, S.; et al. HVSR analysis of seismic site effects and soil-structure resonance in Varaždin city (North Croatia). *Soil Dyn. Earthq. Eng.* **2013**, *92*, 666–677. [CrossRef]
- 32. Mahajan, A.K.; Galiana-Merino, J.J.; Lindholm, C.; et al. Characterization of the sedimentary cover at the Himalayan foothills using active and passive seismic techniques. *J. Appl. Geophys.* **2011**, *73*, 196–206. [Cross-Ref]
- 33. Haefner, R.J.; Sheets, R.A.; Andrews, R.E. Evaluation of the horizontal-to-vertical spectral ratio (HVSR) seismic method to determine sediment thickness in the vicinity of the South Well Field, Franklin County, OH. *Ohio J. Sci.* **2010**, *110*, 77–85.
- 34. Grippa, A.; Bianca, M.; Tropeano, M.; et al. Use of the HVSR method to detect buried paleomorphologies (filled incised-valleys) below a coastal plain: the case of the Metaponto plain (Basilicata, southern Italy). *Boll. Geofis. Teor. Appl.* **2011**, *52*, 225–240. [CrossRef]
- 35. Chandler, V.W.; Lively, R.S. OFR14-01, Evaluation of the horizontal-to-vertical spectral ratio (HVSR) passive seismic method for estimating the thickness of Quaternary deposits in Minnesota and adjacent parts of Wisconsin. Available online: https://hdl.handle.net/11299/162792 (accessed on 4 July 2025).
- 36. Zhu, C.; Cotton, F.; Pilz, M. Detecting Site Resonant Frequency Using HVSR: Fourier versus response spectrum and the first versus the highest peak frequency. *Bull. Seismol. Soc. Am.* **2020**, *110*, 427–440. [CrossRef]
- 37. Yamazaki, F.; Ansary, M.A. Horizontal-to-vertical spectrum ratio of earthquake ground motion for site characterization. *Earth. Eng. Struct. Dyn.* **1997**, *26*, 671–689. [CrossRef]
- 38. Mi, B.; Hu, Y.; Jianghai, X.; et al. Estimation of horizontal-to-vertical spectral ratios (ellipticity) of Rayleigh waves from multistation active-seismic records. *Geophysics* **2019**, *84*. [CrossRef]
- 39. Xu, R.; Wang, L. The horizontal-to-vertical spectral ratio and its applications. *EURASIP J. Adv. Sign. Proc.* **2021**, 75, 1–10. [CrossRef]
- 40. Park, C.B.; Miller, R.D.; Xia, J. Multichannel analysis of surface waves MASW. *Geophysics* **1999**, *64*, 800–808. [CrossRef]
- 41. Park, C.; Ryden, N. Historical overview of the surface wave method. *Symp. Appl. Geophys. Eng. Environ. Prob.* **2007**, *897–909*. [CrossRef]
- 42. Kim, D.-S.; Park, H.-C. Determination of dispersive phase velocities for SASW method using harmonic wavelet transform. *Soil Dyn. Earth. Eng.* **2002**, *22*, 675–684. [CrossRef]
- 43. Kang, S.Y.; Kim, K.-H.; Chiu, J.-M.; et al. Microtremor HVSR analysis of heterogeneous shallow sedimentary structures at Pohang, South Korea. *J. Geophys. Eng.* **2020**, *17*, 861–869. [CrossRef]
- 44. Luzi, L.; Puglia, R.; Pacor, F.; et al. Proposal for a soil classification based on parameters alternative or complementary to Vs,30. *Bull. Earth. Eng.* **2011**, *9*, 1877–1898. [CrossRef]
- 45. Héloïse, C.; Bard, P.-Y.; Duval, A.-M.; et al. Site effect assessment using KiK-net data: part 2—site amplification prediction equation based on f0 and Vsz. *Bull. Earth. Eng.* **2012**, *10*, 451–489. [CrossRef]
- 46. Delgado, J.; Casado, C.P.; Giner, J.; et al. Microtremors as a geophysical exploration tool: applications and limitations. *Pure Appl. Geophys.* **2000**, *157*, 1445–1462. [CrossRef]
- 47. Luzi, L.; Bindi, D.; Franceschina, G.; et al. Geotechnical Site Characterisation in the Umbria-Marche Area and Evaluation of Earthquake Site-Response. *Pure Appl. Geophys.* **2005**, *162*, 2133–2161. [CrossRef]
- 48. Di Giulio, G.; Cultrera, G.; Cornou, C.; et al. Quality assessment for site characterization at seismic stations. *Bull. Earth. Eng.* **2021**, *19*, 463–4691. [CrossRef]
- 49. Nugraheni, A.S.; Setianto, A.; Setiawan, H. Comparison of Vs30 value from microtremor data based on SPT drill test of young Merapi deposits in Opak River, Yogyakarta. *J. Geos. Rem. Sens.* **2024**, *101–110*. [CrossRef]
- 50. Kwak, D.Y.; Stewart, J.P.; Mandokhail, S.J.; et al. Supplementing VS30 with H/V spectral ratios for predicting site effects. *Bull. Seismol. Soc. Am.* **2017**, *107*, 2028–2042. [CrossRef]
- 51. Wagle, K.S. Development of data-driven models to predict VS30 with mHVSR. Master's Thesis, Virginia Polytechnic Institute and State University, Blacksburg, VA, USA, 6 May 2025. Available online: https://hdl.handle.net/10919/134297
- 52. Grutas, R.N.; Serrano, A.T.; Tan, J.M.L.C.; et al. Rapid estimation of Vs30 through elitist genetic algorithm HVSR inversion and refraction microtremor data analysis in the Greater Metro Manila Area and Leyte Province, Philippines. *Appl. Sci.* **2025**, *15*, 2447. [CrossRef]
- 53. Francisco, G.-S.; Mojica, A.; Ho, C.; et al. Horizontal-to-vertical spectral ratios and refraction microtremor analyses for seismic site effects and soil classification in the City of David, western Panama. *Geosciences* **2023**, *13*, 287. [CrossRef]
- 54. Alexopoulos, J.D.; Dilalos, S.; Voulgaris, N.; et al. The contribution of near-surface geophysics for the site

- characterization of seismological stations. *Appl. Sci.* **2023**, *13*, 4932. [CrossRef]
- 55. Ávila-Barrientos, L.; Yegres-Herrera, L.A.; Flores-Estrella, H.; et al. Seismic site conditions of RESNOM network. *Seismica* **2024**, *3*, 1–10. [CrossRef]
- 56. Yong, A.; Martin, A.; Stokoe, K.; et al. ARRA-funded VS30 measurements using multi-technique approach at strong-motion stations in California and central-eastern United States. In *U.S. Geological Survey Open-File Report 2013–1102*; Geological Survey (U.S.): Reston, VA, USA, 2013. Available online: https://pubs.usgs.gov/of/2013/1102/ (accessed on 4 July 2025).
- 57. Gospe, T.; Zimmaro, P.; Wang, P.; et al. Supplementing shear wave velocity profile database with microtremor-based H/V spectral ratios. In Proceedings of the 17th World Conference on Earthquake Engineering, Sendai, Japan, 13 September 2020. Available online: https://escholarship.org/uc/item/49g 807wz
- 58. Odum, J.K.; Stephenson, W.J.; Williams, R.A.; et al. VS30 and spectral response from collocated shallow, active-, and passive-source VS data at 27 sites in Puerto Rico. *Bull. Seismol. Soc. Am.* **2013**, *103*, 2709–2728. [CrossRef]
- 59. Stephenson, W.J.; Yong, A.; Martin, A. Flexible multimethod approach for seismic site characterization. *J. Seismol.* **2022**, *26*, 687–711. [CrossRef]
- 60. Cederberg, J.R.; Gardner, P.M.; Thiros, S.A. Hydrology of northern Utah Valley, Utah County, Utah, 1975–2005. In *Scientific Investigations Report 2008-5197*; Geological Survey (U.S.): Reston, VA, USA, 2009. Available online: https://pubs.usgs.gov/sir/2008/5197/ (accessed on 4 July 2025).
- 61. Stephenson, W.J.; Odum, J.K.; Williams, R.A.; et al. Characterization of intrabasin faulting and deformation for earthquake hazards in southern Utah Valley, Utah, from high-resolution seismic imaging. *Bull. Seismol. Soc. Am.* **2012**, *102*, 524–540. [CrossRef]
- 62. Davis, D.A.; Cook, K.L. Evaluation of low-temperature geothermal potential in Utah and Goshen Valleys and adjacent areas, Utah, part 1 gravity survey. *Utah Geol. Min. Surv. Rep. Invest* **1983**. Available online: https://ugspub.nr.utah.gov/publications/reports_of_investigations/RI-179.pdf (accessed on 4 July 2025).
- 63. Kowallis, B.J.; Wald, L.C. Rock Canyon near Provo, Utah County—a geologic field laboratory. In *Utah Geosites*; Milligan, M., Biek, R.F., Inkenbrandt, P., et al., Eds.; Utah Geological Association: Salt Lake City, CO, USA, 2019; pp. 1–15. [CrossRef]
- 64. Machette, M.N. Surficial geologic map of the Wasatch Fault zone, eastern part of Utah Valley, Utah County and parts of Salt Lake and Juab Counties, Utah. *U.S. Geol. Surv. Misc. Invest. Ser. Map* **1992**. [CrossRef]
- 65. Solomon, B.J.; Constenius, B.K.; Machette, M.N. Interim geologic map of the Orem quadrangle, Utah County, Utah. *Utah Geol. Surv. Open-file Rep.* **2010**, *567*.
- 66. Bissell, H.J. *Lake Bonneville: Geology of Southern Utah Valley, Utah*; U.S. Geological Survey: Washington, D.C., USA, 1963; pp. 1–130.
- 67. Solomon, B.J.; Machette, M.N. Interim geologic map of the Provo 7.5' quadrangle, Utah County, Utah. *Utah Geol. Surv. Open-file Rep.* **2008**, *525*, 31.
- 68. 2014 Seismic Hazard Map- Utah. Available online: https://www.usgs.gov/media/images/2014-seismic -hazard-map-utah (accessed on 4 July 2025).
- 69. NEHRP Recommended Seismic Provisions for New Buildings and Other Structures, Volume I: Part 1 Provisions, Part 2 Commentary FEMA P-2082-1. 2020. Available online: https://nibs.org/wp-content/uploads/2025/04/fema_2020-nehrp-provisions_part-1-and-part-2.pdf (accessed on 4 July 2025).
- 70. National Oceanic and Atmospheric Administration. Available online: https://www.weather.gov/wrh/Climate?wfo=slc (accessed on 20 August 2025).
- 71. Nelson, S.; McBride, J.; Rey, K. The effect of saturation and salts on the rigidity of fine-grained material. *J. Appl. Geophys.* **2023**, *213*, 1–8. [CrossRef]
- 72. Montgomery, D.C.; Peck, E.A.; Vining, G.G. *Introduction to Linear Regression Analysis*, 5th ed.; John Wiley & Sons, Inc.: Hoboken, NJ, USA, 2012; pp. 12–53.
- 73. Stephenson, W.J.; Odum, J.K. Application of the spatial-autocorrelation microtremor-array method for characterizing S-wave velocity in the upper 300 m of Salt Lake Valley, Utah. *Geophys. Dev. Ser.* **2002**, 447–460. [CrossRef]
- 74. Gniazdowska, A. Seismic Surface Wave Surveying of Levees in the Sacramento Delta. Master's Thesis, California State University, East Bay, Hayward, CA, USA, December 2021. Available online: https://hdl.handle.net/20.500.12680/4m90f174j
- 75. Gniazdowska, A.; Craig, M.; Uhlemann, S.; et al. Seismic surface wave surveying of levees in the Sacramento Delta using 1D and 2D active and passive methods. In Proceedings of the American Geophysical Union Fall

- Meeting, New Orleans, LA, USA, 13 December 2021.
- 76. Uhlemann, S.; Ulrich, C.; Gniazdowska, A.; et al. Rapid geophysical characterization of levees internal structure using streamer-based multi-method geophysical approaches. In Proceedings of the American Geophysical Union Fall Meeting, New Orleans, LA, USA, 13 December 2021.
- 77. Bollinger, G.A. Seismicity of the southeastern United States. *Bull. Seismol. Soc. Am.* **1973**, *63*, 1785–1808. [CrossRef]
- Copyright © 2025 by the author(s). Published by UK Scientific Publishing Limited. This is an open access article under the Creative Commons Attribution (CC BY) license (https://creativecommons.org/licenses/by/4.0/).

Publisher's Note: The views, opinions, and information presented in all publications are the sole responsibility of the respective authors and contributors, and do not necessarily reflect the views of UK Scientific Publishing Limited and/or its editors. UK Scientific Publishing Limited and/or its editors hereby disclaim any liability for any harm or damage to individuals or property arising from the implementation of ideas, methods, instructions, or products mentioned in the content.